CALIGULA, A STARDUST SULFIDE-SILICATE ASSEMBLAGE VIEWED THROUGH SEM, NANOFTIR AND STXM.

Zack Gainsforth[1], Alex McLeod[2], Anna Butterworth[1], Gerardo Dominguez[3], Dimitri Basov[2], Fritz Keilmann[4], Mark Thiemens[2], Tolek Tyliszczak[5], Andrew J. Westphal[1] , [1] *Space Sciences Laboratory, University of California at Berkeley, Berkeley CA 94720, USA,* [2] *University of California at San Diego, La Jolla, CA 92093, USA,* [3] *California State University, San Marcos, San Marcos, CA 92096-0001, USA,* [4] *LASNIX, Sonnenweg 32, 82152 Berg, Germany,* [5] *Advanced Light Source, Lawrence Berkeley National Laboratory, Berkeley, CA 94720-8225, USA .*

Introduction

NASA's Stardust mission returned samples from Comet 81/P Wild 2[1], comprising a broad diversity of materials including amorphous condensation products and melt assemblages containing glasses[2]. Characterizing amorphous phases is key to understanding the formation of these primitive solar system constituents. Here we apply a new combination of techniques to examine an amorphous phase in one such Stardust sample, a grain named Caligula.

Use of NanoFTIR

Fourier transform infrared (FTIR) is powerful for studying bond structures, but has limited spatial resolution. In the case of the 10 μm silicate stretch, the diffraction limit is theoretically about 5 μm, but practically close to 10 μm in most cases. Particles returned by NASA's Stardust mission have sub-micron internal structures, so FTIR is difficult to apply. However, scanning near-field optical microscopy, or nanoFTIR[3][4][5] is a relatively new atomic force microscopy, that can probe the infrared optical qualities of samples far below the usual diffraction limit. Just like FTIR, it can potentially map amorphous silicate structures[8]. Spectra are not equivalent to, but can theoretically be related in a one to one fashion with traditional FTIR spectra. In our case we probed the 10 μm silicate stretch with $\approx$ 100 nm spatial resolution. Other promising applications include the examination of carbonaceous and silicate materials in meteorites[6].

Experimental

The largest terminal particle of Stardust track C2035,5,1(5 (named Caligula) is a 12 x 6 μm complex assemblage of pyrrhotite and heterogeneous silicate. It was embedded in epoxy and the top $\approx$ 5 μm was ultramicrotomed into 80 nm thick sections at the National Center for Electron Microscopy (NCEM). The remaining bullet was analyzed by nanoFTIR at the University of California in San Diego (UCSD) using a Neaspec atomic force microscope with a broadband laser from Toptica Photonics tuned to a 300 cm^{-1} bandwidth around the 10 μm silicate stretch (750-1100 cm^{-1}). Difference-frequency generation components were provided by Lasnix.

The bullet was then imaged in a Tescan Vega III scanning electron microscope (SEM) at the University of California at Berkeley (UCB) with an 80mm^2 EDS detector from Oxford. Quantitative EDS maps were taken at 10 keV and 200 pA which gave a spatial resolution of around a few hundred nm, varying by element. Figure 1 shows the SEM backscatter image and an RGB image produced from Ca, Mg and Na SEM/EDS X-ray maps.

The ultramicrotomed slices were imaged using scanning transmission X-ray microscopy (STXM) at the Advanced Light Source (ALS) in Berkeley, CA. Future work will involve TEM analysis of the ultramicrotomed slices at NCEM.

Observations

Pyrrhotite: SEM/EDS shows that the pyrrhotite has composition $Fe_{1-x}S$ where $x < 0.01$ (2σ statistical) relative to Canyon Diablo troilite. Some Si and O are present in the spectrum as well, but could possibly be due to the close proximity of the silicate. Future transmission electron diffraction will

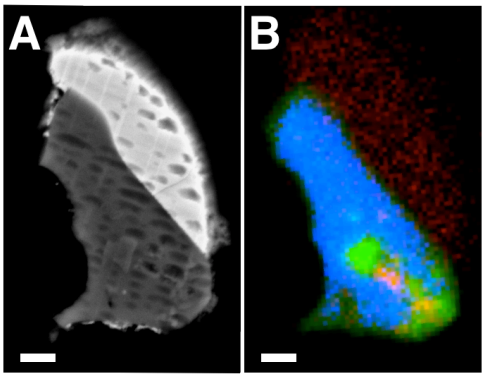

Figure 1: SEM images of Caligula. A) Backscattered electron image taken at 10 keV shows the sulfide in the upper right, and silicate in the lower left. B) Tricolor plot made from EDS maps for Ca (red), Mg (green), and Na (blue). The Brehmstrahllung in the Ca channel (red) shows the outline of the sulfide. There is no Ca in the sulfide. Scalebars are 1 μm.

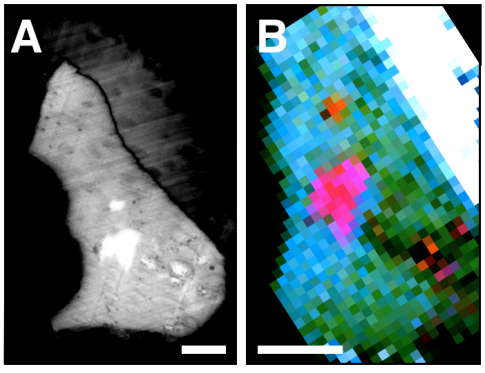

Figure 2: NanoFTIR images of Caligula. A) Whitebeam optical image showing phases and phase boundaries in the infrared. B) Tricolor image constructed from three frames of a spectrum image. Red is the 940 cm^{-1} frame, green is 993.33 cm^{-1}, and blue is 1043.33 cm^{-1}. The pixels are 100 nm in width. Scalebars are 1 μm.

determine the presence or absence of a pyrrhotite superlattice.

Non-stoichiometric silicate matrix: The silicate assemblage comprises a non-stoichiometric matrix with nanophase inclusions. The matrix composition is (At %): O = 60.85, Na = 6.52, Mg = 5.59, Al = 0.51, Si = 23.62, P = 0.63, S = 0.11, K = 0.19, Ca = 0.22, Mn = 0.52, Fe = 1.22. The most variable element is Na which varies down to 5.80 At %. An Mg K-edge XANES spectrum acquired by STXM shows almost no structure, with a single 10 eV wide resonance enhancement that has an optical density only $\approx$ 20% higher than the edge jump. No EXAFS oscillations are visible in the subsequent 100 eV. Otherwise, the spectrum looks close to a theoretical hydrogenic model[7]. As described, the Mg XANES spectrum is strongly suggestive of an amorphous coordination environment for the Mg cation. NanoFTIR shows a peak at 950 cm^{-1} on the side furthest from the sulfide (green region in Figure 2B), while a peak at 1040 cm^{-1} is present everywhere but lower in intensity away from the sulfide. In both cases, the FTIR peaks are broad and poorly resolved, which is consistent with the hypothesis that the phase is amorphous.

Pyroxene: The largest silicate inclusion is $\approx$ 1 μm across (green in Figure 1B, red in Figure 2B). It is euhedral with (At %): O = 60.41, Na = 1.75, Mg = 15.05, Si = 21.68, Ca=0.67, Fe=0.44. The composition matches enstatite with minor Ca and Na ($\approx En_{93}Wo_3Ae_4$). Mg K-edge XANES going 100 eV beyond the edge gives a spectrum with three distinct resonance enhancements. The central peak is at 1314 $\pm$1 eV, with relative peaks at $\Delta E = -4.2$ and +4.8 eV, and two EXAFS oscillations, which compares favorably against an enstatite standard. The nanoFTIR spectrum shows two strong, well defined peaks at 950 cm^{-1} and 1060 cm^{-1} and a weaker peak at 1010 cm^{-1}.

NanoFTIR Acquisition

Figure 2A shows a white beam image of Caligula produced without acquiring a spectrum, but instead using the full bandwidth of the laser (in this case about 300 cm^{-1}). This method allows fast acquisitions with excellent contrast. However, the resulting image is not quantitative except in determining phase locations and boundaries.

Figure 2B is an RGB image produced from three energies in a spectral stack containing 68 energies spanning 850-1073 cm^{-1}. The entire stack required about 6 hours to complete and was acquired during a period of exceptional laser stability. The image is skewed slightly due to drift in the nano positioning stage over the 6 hour acquisition, but corresponds to the bottom half of Figure 2A.

The three energies were chosen to maximize contrast between the phases involved. The 1040 cm^{-1} peak (blue) is present in the non-stoichiometric silicate matrix but is off resonance for the pyroxene inclusion, and mostly tracks the matrix. The 940 cm^{-1} peak (red) is present in both the matrix and the pyroxene inclusion, but is very much more intense in the inclusions, hence they are red. The 993 cm^{-1} peak (green) resides in a minima between the 940 and 1043 cm^{-1} peaks, and therefore provides good contrast for variations in the matrix without being swamped by the 940 cm^{-1} peak found in the inclusions. The pyrrhotite is reflective in IR and shows white.

In Figure 2B, we can clearly see a gradient in the matrix showing the gradual variation in the silicate character from one side of the grain to the other. It is seen as a variation from blue to green as the 1040 cm^{-1} (blue) peak intensity varies. Comparison against the EDS map in Figure 1B shows that the silicate is varying in the region containing sub-micron inclusions as well as a region without inclusions. Therefore, it appears to be tracking a property of the matrix itself.

Integrating methods

The combination of SEM/TEM, STXM, and nanoFTIR are necessary to understand amorphous silicates in Stardust. SEM/TEM provides characterization of the material and identification of related crystallites.

STXM provides ordering information of many cations and the structural elements silicon, oxygen and aluminum. Here, we saw in the Mg XANES that there was no clear order around the Mg cations in the non-stoichiometric silicate matrix.

Like FTIR, nanoFTIR appears to provide a very sensitive tracer of silicate structure making the ordering process visible before cation ordering becomes visible in XANES spectra. In the matrix, the silicate stretch contained two peaks whose positions did not change, but whose intensities did. While we cannot interpret this quantitatively yet, we know at least that there is a variability from one side of the particle to the other, even though the Mg ordering has not occurred. Thus conjunction of STXM and nanoFTIR data provides the relative ordering sequence of elements in the glass.

Future work

Caligula appears to be a complex assemblage of amorphous silicate with pyroxene inclusions and possibly other silicate inclusions in close association with a large sulfide and likely fine grained sulfides as well. Further TEM analysis should elucidate the identity and crystallinity of the phases and allow more quantitative analysis of both the XANES and nanoFTIR results. Once this is accomplished, we hope to form a plausible formation mechanism for Caligula in the context of its cometary history and/or condensation processes, etc.

Acknowledgments

UCB/SSL funded by a NASA Stardust Participating Scientist grant. The UCSD effort was supported by NASA LARS grant NNX11AF24G. The ALS and NCEM are is supported by the Director, Office of Energy Research, Office of Basic Energy Sciences, Materials Sciences Division of the U.S. Department of Energy, under Contract No. DOE-AC03-76SF00098.

References

[1] Brownlee, D. E., et. al., (2006) *Science*, 314, 1711. [2] Joswiak, D., et. al., (2012) *Meteoritics & Planet. Sci.*, 47, 471. [3] Keilmann, F., Hillenbrand, R., (2004) *Phil. Trans. R. Soc. A*, 362, 787-805. [4] Keilmann, F., Amarie, S., (2012) *J. Infrared Milli. Terahz Waves*, 33, 479-484. [5] Amarie, S., Keilmann, F., (2011) *Phys. Rev. B*, 83, 45404. [6] McLeod, A. S., et al, (2013) *44th LPSC*, submitted. [7] Egerton, R. F., (1996) 2nd ed., Plenum Press. [8] Mutschke, H., (1998) *Astron. Astrophys.*, 333, 188-198